PHYSICAL REVIEW B VOLUME 57, NUMBER 12 15 MARCH 1998-II

Transport and reactions of gold in silicon containing cavities

S. M. Myers and G. A. Petersen
Sandia National Laboratories, Albuquerque, New Mexico 87185-1056
(Received 21 July 1997; revised manuscript received 20 November 1997)

We quantified the strength of Au binding on cavity walls and in precipitates of the Au-Si molten phase within Si over the temperature range 1023–1123 K. Also determined was the diffusivity-solubility product of interstitial Au. These properties were obtained by using ion implantation and annealing to form multiple layers containing cavities or Au-Si precipitates and then measuring by Rutherford backscattering spectrometry the rate and extent of Au redistribution between layers during isothermal heating. Results were incorporated into a diffusion-reaction formalism describing the evolution of the coupled concentrations of interstitial Au, substitutional Au, Si interstitial atoms, and Si vacancies. Cavities were shown to be effective sinks for the gettering of Au from solution in Si. [S0163-1829(98)04911-X]

I. INTRODUCTION

The transport and reactions of Au in Si have been widely investigated for a variety of reasons. This solute is prototypical of transition metals that occupy both interstitial and substitutional lattice sites within Si, and measurement of its transport serves to illuminate the less readily observed diffusion of Si self-interstitial atoms.[1–7] In devices, deep electronic levels associated with substitutional Au are sometimes exploited to reduce carrier lifetimes, whereas in other circumstances, with the Au present as a trace impurity, the same deep levels are highly detrimental.[8] Because of the latter effect, many investigators have studied the gettering of Au to controllably introduced sinks within Si; the examined gettering centers include SiO_2 precipitates and associated defects,[9] in-diffusing phosphorus,[10,11] ion-implantation damage and implanted impurities,[12–15] and cavities formed by implantation of hydrogen or helium and annealing.[16–19] Finally, Au reacts strongly with the unoxidized surface of Si, producing complex reconstructions, and these reconstructions have been extensively investigated on external surfaces following vapor deposition of Au in ultrahigh vacuum. (See, e.g., Refs. 20–30 and citations therein.)

In the present work, we examined the behavior of ion-implanted Au in Si that contained nanometer-size cavities formed by He ion implantation and annealing. Rutherford backscattering spectrometry (RBS) was used to measure the rate and equilibrium extent of two internal redistributions of the Au: first, from precipitates of the equilibrium Au-Si phase to cavities; and, second, from one cavity layer to another. Resulting data were analyzed to obtain the binding free energies of Au chemisorbed on the cavity walls and contained within the Au-Si phase relative to Au in interstitial solution within the Si lattice. This served to quantify the strength of a potentially important gettering reaction. Moreover, by illuminating the energetics of chemisorbed Au relative to bulk solution and to the three-dimensional Au-Si phase, these studies provided fundamental information not readily obtained from earlier studies of deposited Au on external surfaces. Finally, the present ion-beam experiments determined the diffusivity-solubility product of interstitial Au in a more direct manner and at lower temperatures than was previously done.

The behavior of the Au was modeled using a formalism that describes the diffusion and coupled transformations of interstitial Au, substitutional Au, interstitial Si, and vacancies in addition to treating the binding reactions of Au at cavities and at Au-Si precipitates. Our analysis included two chemisorption states on the cavity walls, with the relative occupancies of these states depending upon coverage. The modeling was used first to interpret and analyze our observations. It was then employed to confirm the consistency of our parametrizations with earlier, higher-temperature experiments that measured depth profiles of substitutional Au resulting from the in-diffusion of interstitial Au and its exchange with substitutional Si.[2] Having thus tested the utility of the model, we used it to examine the efficacy of cavities as sinks for the gettering of Au from solution in Si.

This quantitative investigation of Au interactions with cavities builds upon the work of Refs. 16–18, which established important aspects of the behavior of the system. Preliminary results from the present study were reported previously.[19]

II. APPROACH

The principal objective of our experiments was to determine quantitatively the strengths of Au binding at cavity walls and within the equilibrium precipitated Au-Si phase relative to mobile interstitial Au in solution. To this end, we ion-implanted He and Au into Si and then annealed to form multiple layers containing either nanometer-size voids or Au-Si precipitates; considerations relating to the creation of these microstructural features have been detailed elsewhere.[16,31,32] Rutherford backscattering spectrometry was then used to observed the redistribution of Au between the layers during isothermal vacuum annealing at 1023, 1073, and 1123 K. At these temperatures, the equilibrium Au-Si precipitated phase is molten with a reported Au content between 60 and 70 at. %.[33] Both the rate and the equilibrium extent of the Au redistributions are related to the binding strengths of interest, and this is the basis of our determination of these quantities. In the remainder of this

0163-1829/98/57(12)/7015(12)/$15.00 © 1998 The American Physical Society

section, we describe the mathematical formulation of the above relationships and outline more specifically the experiments that were carried out to exploit them. The discussion initially uses simplifying approximations to convey the underlying physical concepts, and then turns to the more elaborate mathematical formalism actually used to model the behavior of the system.

A. Simplified treatment of interlayer redistribution

In the case of two layers of negligible width that are exchanging Au by steady-state diffusion, the interlayer atomic flux Φ is given by

$$\Phi=([\mathrm{Au},i]_1-[\mathrm{Au},i]_2)N_{\mathrm{Si}}D_{\mathrm{Au},i}/\Delta x, \qquad (1)$$

where $[\mathrm{Au},i]$ is the atomic fraction of mobile interstitial Au in local equilibrium with the bound state in layer 1 or 2, N_{Si} is the atomic density of Si, $D_{\mathrm{Au},i}$ is the diffusion coefficient of interstitial Au, and Δx is the separation of the layers. When the system eventually comes to full equilibrium,

$$[\mathrm{Au},i]_1=[\mathrm{Au},i]_2. \qquad (2)$$

The binding strengths of interest are directly related to the $[\mathrm{Au},i]$. For example, when the bound state is the equilibrium Au-Si phase, the corresponding concentration is simply the thermodynamic solubility,

$$[\mathrm{Au},i]_{\mathrm{AuSi}}=\exp(-\Delta G_{\mathrm{AuSi}}/kT). \qquad (3)$$

In this paper, ΔG is defined as

$$\Delta G=\Delta H-T\Delta S_{\mathrm{ex}}, \qquad (4)$$

where ΔH is the enthalpy change when one Au atom moves from the bound state to interstitial solution and ΔS_{ex} is the corresponding change in excess entropy. The latter quantity is defined more specifically as the excess entropy difference after configurational contributions arising from the occupation of multiple solution sites and multiple cavity-wall sites are taken into account separately and explicitly. In the usage of thermodynamics, ΔG might be termed a relative partial excess atomic Gibbs free energy of solution; we refer to it simply as the binding free energy.

For the case where Au bound within a layer occupies cavity-wall chemisorption sites, we consider two regimes, one of low wall coverage and the other of high coverage; our treatment of both of these is simplified to the greatest degree compatible with the experimental data presented in Sec. IV. The chemisorption sites are assumed to be saturable, fixed in number, and of a single type. When the average fractional occupation of the sites, θ, is below a threshold value θ_t that depends only on temperature, the sites are taken to be noninteracting and randomly occupied; consequently, the chemisorbed Au behaves as a two-dimensional lattice gas. The locally equilibrated solution concentration is then given by

$$[\mathrm{Au},i]_{\mathrm{cav}}=\{\theta/(1-\theta)\}\exp(-\Delta G_{\mathrm{rc}}/kT) \quad \text{for } \theta\leqslant\theta_t, \qquad (5)$$

where ΔG_{rc} is the binding free energy associated with the random chemisorption. For $\theta>\theta_t$, the surface is taken to be in a two-phase condition, with regions of random chemisorption coexisting with ordered islands of chemisorbed atoms. Ordering of Au has been directly observed on external Si surfaces,[20–30] and, as discussed in Sec. IV, our findings point to its occurrence on cavity walls. When the two-phase condition is present, the chemical potential of the Au is independent of the average wall coverage θ, and

$$[\mathrm{Au},i]_{\mathrm{cav}}=\exp(-\Delta G_{\mathrm{oc}}/kT) \quad \text{for } \theta\geqslant\theta_t, \qquad (6)$$

where ΔG_{oc} is the binding free energy for the ordered chemisorption. Combining Eqs. (5) and (6) with $\theta=\theta_t$ yields the relationship

$$1/\theta_t=1+\exp\{(\Delta G_{\mathrm{oc}}-\Delta G_{\mathrm{rc}})/kT\}. \qquad (7)$$

The equilibrium three-dimensional Au-Si phase described by Eq. (3) is expected to precipitate in cavities when the adjacent solution concentration exceeds the equilibrium solubility, and such precipitation has in fact been observed.[17,18] In the present experiments, however, this unwanted complication was suppressed by using either of two procedures: in one, the Au-Si phase was formed by Au implantation and annealing before the introduction of cavities, so that the solution was not supersaturated during subsequent gettering to the cavities; in the other procedure, the total quantity of introduced Au was restricted to an amount less than could be accommodated by the energetically favored submonolayer chemisorption on the cavity walls. Our experimental results indicate that these steps were successful, as will be discussed in Sec. IV.

The simplicity of Eqs. (5)–(7) is achieved through substantial simplification of the probably complex interactions of Au with internal cavity surfaces. For instance, while the predominant facet on the cavity walls has (111) orientation, (100) and (110) facets are also present, and curved regions are observed as well.[32,34,35] Moreover, at least four types of ordering have been reported for the (111) orientation alone, although this situation becomes simpler at temperatures above about 1000 K (See, e.g., Ref. 30.) Hence, multiple types of ordered chemisorption may conceivably occur on the cavity walls. Our treatment of random chemisorption at low coverage is also approximate, since more than one surface orientation is present in reality and since direct or reconstruction-mediated interactions among the Au atoms may not be negligible as assumed. While it would be straightforward in principle to incorporate all of these effects into the formalism by replacing Eqs. (5)–(7) with a generalized function of the form $[\mathrm{Au},i]=f(\theta,T)$, this is not justified by the information currently available, in our view. As matters now stand, such an elaboration would be attended by a multiplication of parameters without independently known values. It is therefore more illuminating, we believe, to employ the simplified model and consider the extent and nature of its deviation from experiment.

B. The experiments and their rationale

Making use of Eqs. (1)–(7), we now consider the kinds of experiments that can be expected to determine ΔG_{AuSi}, ΔG_{rc} and ΔG_{oc}. The most straightforward condition to interpret is one of equilibrium among the interacting layers, which is described by Eq. (2) with appropriate substitutions from Eqs. (3), (5), and (6). We previously used this method

to evaluate $\Delta G_{\rm rc}$ for Fe and Co on cavity walls.[36] In those experiments, a cavity layer of known internal-surface area was allowed to equilibrate with a separate layer containing a large excess of metal-silicide phase with a known value of ΔG. The value of θ for the cavities was then measured, permitting the binding free energy of interest to be extracted using Eqs. (2), (3), and (5). In the present studies of Au, however, analogous experiments yielded $\theta \approx 1$, corresponding to saturation of the cavity walls. This serves to demonstrate that $\Delta G_{\rm oc} \gtrsim \Delta G_{\rm AuSi}$, but it does not determine the value of either quantity. Furthermore, equilibrium between two cavity layers or between two layers with Au-Si precipitates is also not illuminating.

Having reached these negative conclusions, we are left with the time dependence of the amounts of Au in the interacting layers as the experimentally accessible property that can quantify the binding free energies of interest. For example, when a layer containing Au-Si precipitates gives up Au to a nearby layer of cavities with much stronger binding, the above equations yield

$$\Phi = [{\rm Au},i]_{\rm AuSi} N_{\rm Si} D_{{\rm Au},i}/\Delta x = \exp(-\Delta G_{\rm AuSi}/kT) N_{\rm Si} D_{{\rm Au},i}/\Delta x. \quad (8)$$

Similarly, for redistribution between two cavity layers where the wall occupancies are both less than θ_t,

$$\Phi = \{\theta_1/(1-\theta_1) - \theta_2/(1-\theta_2)\} \times \exp(-\Delta G_{\rm rc}/kT) N_{\rm Si} D_{{\rm Au},i}/\Delta x. \quad (9)$$

Here the redistribution occurs even though $\Delta G_{\rm rc}$ is the same for the two layers because of the dependence of the configurational component of entropy on θ for the two-dimensional lattice gas. Finally, when the redistribution is from a cavity layer with $\theta > \theta_t$ to a cavity layer with $\theta < \theta_t$,

$$\Phi = [\exp(-\Delta G_{\rm oc}/kT) - \{\theta_2/(1-\theta_2)\} \times \exp(-\Delta G_{\rm rc}/kT)] N_{\rm Si} D_{{\rm Au},i}/\Delta x. \quad (10)$$

With an independently evaluated diffusion coefficient, these three experiments serve to determine $\Delta G_{\rm AuSi}$ $\Delta G_{\rm rc}$, and $\Delta G_{\rm oc}$. This was the approach taken in the present experiments.

An important feature of the above interlayer fluxes is that they depend on the products of Boltzmann factors such as $\exp(-\Delta G_{\rm AuSi}/kT)$ and the diffusion coefficient $D_{{\rm Au},i}$, so that knowledge of the diffusivity is required to extract the binding free energies from the experimental data. To our knowledge, $D_{{\rm Au},i}$ has not been precisely determined. An experimentally based estimate is available, however, and it is similar to results for interstitial Cu and Ni; the activation energies for the three elements are 0.39, 0.43, and 0.47 eV, respectively, and the corresponding prefactors are 0.024, 0.47, and 0.20 mm^2/s.[37–40] In analyzing the experimental data, we employed a representative diffusion coefficient of $D_{{\rm Au},i} = (0.10\ {\rm mm}^2/{\rm s})\exp(-0.4\ {\rm eV/kT})$, and the resultant binding free energies are reported instead of the more directly determined products of the diffusivity and the Boltzmann factors. Since even an order-of-magnitude error in the diffusion coefficient would translate into a shift of only about 0.2 eV in the extracted binding free energies, or $\sim 10\%$, and since relative magnitudes would be unaffected, this step was considered to be warranted in light of the considerable simplification of the discussion. Moreover, revision in the light of future diffusion results would be trivially accomplished. We nevertheless present values of $N_{\rm Si}$ $[{\rm Au},i]_{\rm AuSi}$ $D_{{\rm Au},i}$ because of the practical importance of this particular product in controlling the uptake of Au into Si.

C. A more comprehensive description of Au transport and reactions

The discussion to this point has ignored the well established, reversible conversion of Au interstitial atoms to immobile, substitutional Au.[1–7] This effect can occur either through exothermic reaction with a vacancy,

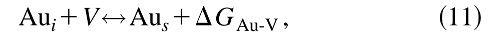

$$\mathrm{Au}_i + V \leftrightarrow \mathrm{Au}_s + \Delta G_{\text{Au-V}}, \quad (11)$$

or by the endothermic kick-out mechanism,

$$\mathrm{Au}_i + \mathrm{Si}_s + \Delta G_{\text{Au-}I} \leftrightarrow \mathrm{Au}_s + I, \quad (12)$$

where the subscript i denotes interstitial sites, s refers to substitutional sites, V is the Si vacancy, I is the Si self-interstitial atom, and $\Delta G_{\text{Au-}V}$ and $\Delta G_{\text{Au-}I}$ are positive binding free energies defined in analogy with Eq. (4). The vacancies and interstitials are also subject to mutual annihilation,

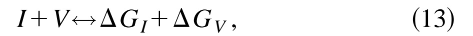

$$I + V \leftrightarrow \Delta G_I + \Delta G_V, \quad (13)$$

where ΔG_I is the Gibbs-free-energy change associated with the creation of a self-interstitial at a specified site and ΔG_V is the corresponding quantity for the vacancy. When Au moves from a near-surface source into the underlying Si bulk, the kick-out process of Eq. (12) is generally found to predominate.[1–7]

In the case of the present experiments, which employed annealing temperatures $\leqslant 1123$ K, simple considerations suggest that the formation of immobile substitutional Au should not have importantly influenced the observed interlayer redistributions. In particular, the solubility of substitutional Au in equilibrium with the Au-Si phase at 1123 K is $N_{\rm Si}[{\rm Au},s]_{\rm AuSi} = 1.5\times10^{15}\ {\rm cm}^{-3}$,[40] which represents an upper bound on $[{\rm Au},s]$ for our experiments. Hence, within the 0.025 cm thickness of the Si specimens, the depth-integrated areal density of Au atoms was $< 0.4\ {\rm nm}^{-2}$. In comparison, the areal densities of Au undergoing interlayer redistribution ranged from 1.5 to 30 nm^{-2}. Since the number of Au atoms moving to the cavity sinks was substantially larger than the number that might have gone into substitutional solution, the influence of the substitutional component on the redistribution should have been correspondingly small. In presenting this conclusion, however, we emphasize the limitations of its applicability. The amount of substitutional Au in equilibrium with the Au-Si phase increases rapidly with temperature, and calculations indicate that effects on experiments of the type presented here become important below 1300 K. Furthermore, the substitutional state of the Au is central to its influence on electrical properties.

In theoretically treating the behavior of Au, we elected to carry out a full, numerical solution of the diffusion-reaction equations governing the interrelated behaviors of interstitial Au, substitutional Au, Si self-interstitials, and Si vacancies

rather than using the simplified relationships developed in Secs. II A and II B. The employed formalism encompasses the processes given by Eqs. (11)–(13) as well as the Au trapping and precipitation reactions underlying Eqs. (3), (5), and (6), and it avoids the approximations of steady-state diffusion and negligible layer width embodied in Eqs. (1) and (8)–(10). This more complete treatment served to confirm that the neglect of substitutional-Au formation and the other approximations are, in fact, fairly well justified for the particular conditions of our experiments. Moreover, it facilitated a consideration of the broader implications of our findings for circumstances where the approximations are not applicable, notably including conditions relevant to gettering in Si electronic devices. The details of the formalism, the evaluation of parameters not determined by the present experiments, and the method of solution are discussed in the Appendix. Apart from the aspects dealing with Au reactions at the cavities, our mathematical treatment generally parallels one reported previously.[6]

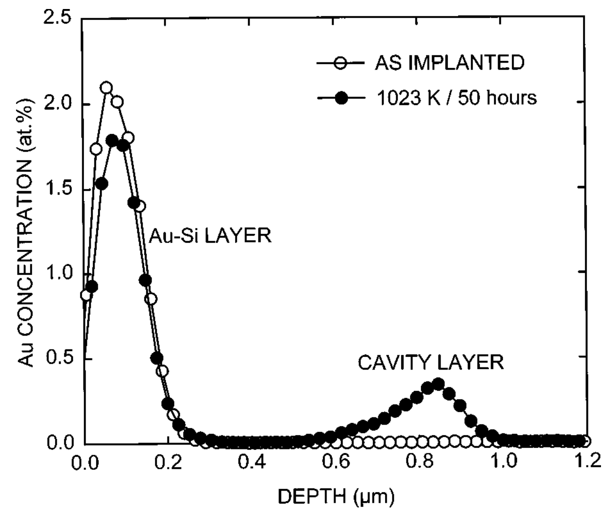

FIG. 1. Depth profiles showing redistribution of Au from a layer containing Au-Si precipitates to a cavity layer.

III. EXPERIMENTAL DETAILS

The samples were of float-zone Si with a room-temperature resistivity $>1\ \mathrm{k}\Omega\ \mathrm{cm}$. The surface orientation was (111) with one face being polished, and the thickness was 0.25 mm. Ion implantations of He and Au were carried out at room temperature in chambers that were turbomolecular pumped to a background pressure of $\sim 10^{-5}$ Pa ($\sim 10^{-7}$ Torr). Vacuum anneals were performed in a quartz furnace tube that was continuously ion-pumped to a pressure of approximately 3×10^{-5} Pa (2×10^{-7} Torr). These anneals were initiated by moving a thermally equilibrated tubular furnace over the evacuated tube and were terminated by withdrawing the furnace, the latter action occupying ~ 2 s. Rutherford backscattering analysis was carried out with ^{4}He at an energy of 2.5 MeV, and the concentration-versus-depth profile of Au was extracted[41] using reported He stopping powers in Si.[42] The possible influence of the analysis beam on the evolution of the depth profile during a sequence of anneals was examined by occasionally making measurements at a new location on the sample; no such effects were found.

IV. RESULTS AND ANALYSIS

A. Redistribution from Au-Si precipitates to cavities

The depth profiles in Fig. 1 exhibit redistribution of Au from an implanted layer containing Au-Si precipitates to an initially unoccupied cavity layer located at a greater depth within the specimen. This sample was first ion-implanted with Au at room temperature to a dose of 160 nm^{-2} using an energy of 300 keV. Then, before the formation of cavities, the specimen was vacuum-annealed at 1123 K for 1 h to induce precipitation of the equilibrium Au-Si phase. This step was taken to avoid a possible transient of nonequilibrium with an attendant supersaturation of solution during the subsequent interlayer redistribution. That the treatment was sufficient to produce the desired precipitation is shown by earlier studies using transmission electron microscopy (TEM), where 100 min at 1123 K was found to cause Au-Si formation even for an implanted Au dose one order of magnitude smaller than used here.[16] The precipitation anneal in the present experiment was followed by implantation of He at room temperature; the dose was 1000 nm^{-2} and the energy 150 keV, leading to a concentration peak near 0.8 μm. Finally, an isothermal series of vacuum anneals was carried out at 1023 K, with the Au depth profile being monitored by RBS. Earlier work showed that cavities form and most of the He diffuses from the specimen in less than 30 min at this temperature, with the subsequent microstructural evolution of the cavities being slow.[31,32]

In Fig. 2, the areal density of Au within the cavity layer of Fig. 1 is shown as a function of anneal time at 1023 K. Also shown are data for two additional redistribution-anneal sequences, one at 1073 K and the other at 1123 K, that were carried out on specimens otherwise treated identically to the first sample. In each case, the transfer is seen to progress until an abrupt saturation at an areal density near 30 Au/nm^2. It is instructive to compare this saturation level with the areal density corresponding to monolayer coverage of the cavity walls; from detailed TEM studies, the latter quantity is 47 nm^{-2} for a cavity formation anneal of 30 min at 973 K,

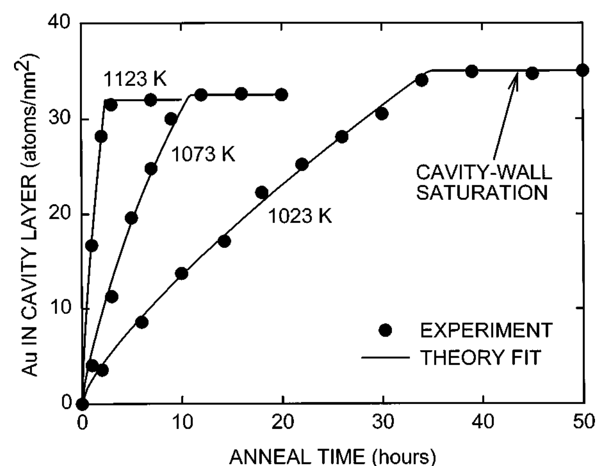

FIG. 2. Redistribution of Au from a layer containing Au-Si precipitates to a cavity layer during annealing at three temperatures. Representative depth profiles are shown in Fig. 1.

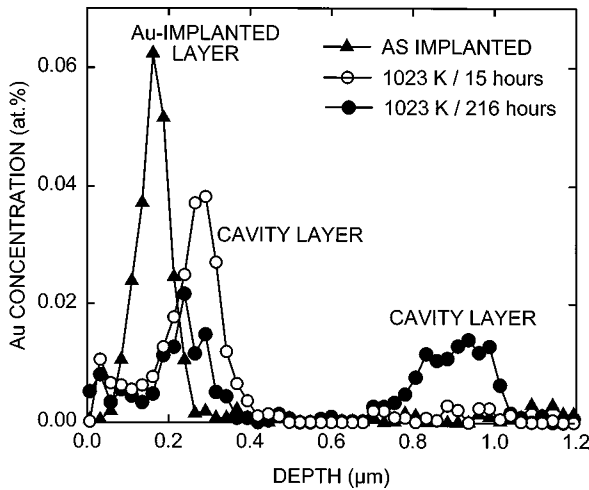

FIG. 3. Depth profiles showing redistribution of Au from one cavity layer to another for an implanted Au dose of 3 nm^{-2}.

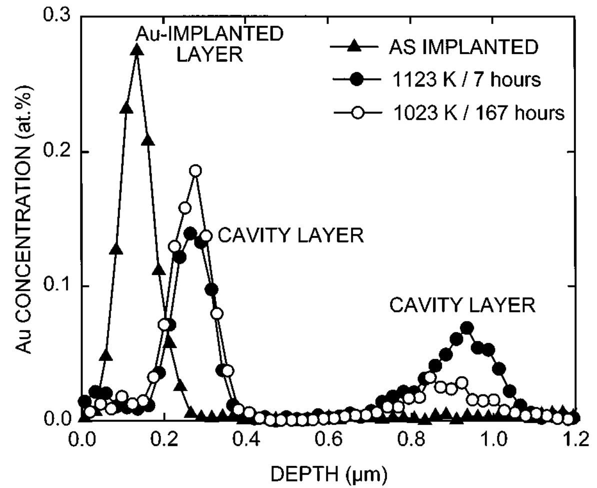

FIG. 4. Depth profiles showing redistribution of Au from one cavity layer to another at two temperatures for an implanted Au dose of 14 nm^{-2}.

32 nm^{-2} for an anneal of 8 h at 1073 K, and 26 nm^{-2} for 1 h at 1173 K.[32] We infer that cavity-wall saturation occurs when the Au coverage reaches approximately 1 monolayer; the observed modest variation of the final areal density among the specimens in Fig. 2 may then result from differences among the cavity microstructures at the three temperatures. A feature of our experiments that leads to such saturation behavior is believed to be the formation of Au-Si phase before the introduction of the cavities; by thereby avoiding supersaturation of solution during the redistribution anneals, the nucleation and growth of the bulk Au-Si phase within the cavities is suppressed. In earlier cavity-gettering studies that encompassed the metastable condition before precipitation of the implanted Au, Au-Si precipitation in the cavities was pronounced.[17,18]

The fact of Au redistribution from the Au-Si phase to the cavities indicates that the binding at the cavities has comparable or greater strength. As discussed in Sec. II B, a more quantitative conclusion requires analysis of the measured interlayer flux; this flux is related to the diffusivity-solubility product $N_{Si}\,[\mathrm{Au},i]_{\mathrm{AuSi}}\,D_{\mathrm{Au},i}$, and thereby to the binding free energy ΔG_{AuSi}, as given approximately by Eq. (8). In Sec. IV C, we will make use of this relationship to extract the diffusivity-solubility product and the binding energy. [The curvature of the plots in Fig. 2 prior to saturation, reflecting a varying interlayer flux not in accord with Eq. (8), is due primarily to the interlayer diffusion distance not being single-valued; this curvature will be seen to conform to the more detailed model calculations.]

B. Redistribution from one cavity layer to another

Figures 3 and 4 show the evolution of Au concentration profiles in Si specimens containing two cavity layers; the cavity distributions were centered at depths of about 0.3 and 0.9 μm, respectively, with the Au-implanted layer lying near 0.15 μm. Of primary interest here is the diffusive redistribution of Au from one cavity layer to another, which illuminates the strength of Au binding at the cavities according to Eqs. (9) and (10). In order to promote constancy of the cavity microstructure during this redistribution, the cavities were formed before the introduction of Au at a temperature higher than those of the redistribution anneals. Helium was implanted at both 30 and 180 keV, the dose being 1000 nm^{-2} in each case, and the specimens were then vacuum-annealed at 1173 K for 1 h. Gold was subsequently injected at 300 keV to one of two nominal doses, 3 or 14 nm^{-2}; these particular doses were chosen to exhibit the cavity-wall binding over a wide range of coverages while maintaining $\theta<1$. After the implantation of Au, the interlayer redistributions were induced by isothermal series of vacuum anneals at 1023, 1073, and 1123 K. It may be noted that, by employing this particular sequence and using relatively small Au doses, we forwent the assurance of early Au-Si precipitation and the resultant absence of solution supersaturation that were emphasized in Sec. IV A. In this situation, however, the possible consequence was simply to hasten the accumulation of Au in the first cavity layer prior to the redistribution between cavity layers; moreover, the relatively small amount of Au could be fully accommodated at cavity-wall chemisorption sites without formation of the less stable Au-Si phase in the cavities. Hence, there should have been no consequences adverse to the objectives of the experiments.

The simplest redistribution behavior was observed at the lower Au dose of 3 nm^{-2}. As seen in Fig. 3, the Au first moved relatively rapidly from the depth of its initial implantation to the nearby cavity layer at 0.3 μm. Then, during more extended annealing sufficient to approach an asymptotic condition, it redistributed between the two cavity layers until an approximately equal partition was reached. Such equal partitioning is consistent with the final state predicted by Eqs. (2) and (5). Equation (5) should apply when the cavity-wall fractional coverage θ is $<\theta_t$, and since in this instance the final state corresponds to $\theta\sim 0.05$, the result is not unexpected.

When similar experiments were carried out with the higher Au dose of 14 nm^{-2}, the final partition of Au between cavity layers departed from equality, by an amount that varied with temperature. This is seen in Fig. 4, where depth profiles after annealing at 1023 and 1123 K for times sufficient to reach the asymptotic condition are shown. While for the higher temperature the amounts of Au in the two cavity

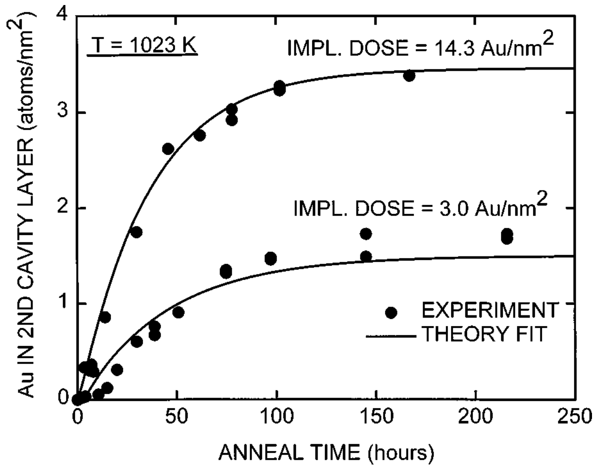

FIG. 5. Redistribution of Au from one cavity layer to another at 1023 K. Representative depth profiles appear in Figs. 3 and 4.

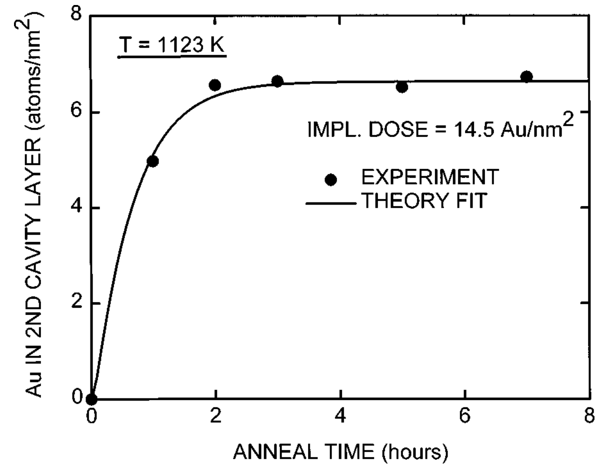

FIG. 7. Redistribution of Au from one cavity layer to another at 1123 K.

layers are approximately equal, there is a pronounced imbalance at the lower temperature.

Within the context of the simplified picture of Sec. II, we hypothesize that the above imbalance results from ordering of the chemisorbed Au atoms on the cavity walls above a threshold coverage θ_t, as discussed in Sec. II A. The proposed scenario is as follows. Early in the anneal sequence when the Au resides almost entirely in the first cavity layer, $\theta_1 \sim 0.5$. This value is assumed to be $>\theta_t$, so that ordered islands of chemisorbed Au atoms coexist with areas of random chemisorption on the cavity walls. In the second cavity layer, $\theta_2 \sim 0 < \theta_t$, implying no ordering. Consequently, from Eqs. (5) and (6), $[\mathrm{Au},i]_1 = \exp(-\Delta G_{\mathrm{oc}}/kT)$ and $[\mathrm{Au},i]_2 \sim 0$. With further annealing, the difference between $[\mathrm{Au},i]_1$ and $[\mathrm{Au},i]_2$ drives the diffusion of Au to the second layer in accord with Eq. (10). This redistribution continues, with a concomitant rise in $[\mathrm{Au},i]_2$ according to Eq. (5), until θ_2 reaches θ_t, whereupon $[\mathrm{Au},i]_1 = [\mathrm{Au},i]_2$ and the redistribution stops. In this final condition, the first cavity layer has both ordered and random chemisorption, while the second layer has only the random state and hence less Au. While this interpretation is inferential, it is reinforced by the following considerations: (1) as already noted, the occurrence of ordered Au chemisorption is well known from studies of external Si surfaces;[20–30] (2) since in the expression for Gibbs free energy the entropy is multiplied by temperature, higher-entropy states such as that of random chemisorption are increasingly favored at higher temperatures, so that θ_t, and hence the amount of Au going to the second cavity layer, should increase with temperature, as seen in Fig. 4; (3) when the total amount of introduced Au is reduced to the point where both θ_1 and θ_2 are less than θ_t, the asymptotic imbalance between layers should disappear, as is observed in Fig. 3. These consistencies lead us to believe that the above picture represents a first approximation to physical reality, albeit one that substantially simplifies the complex behavior of Au on the cavity walls as discussed in Sec. II A.

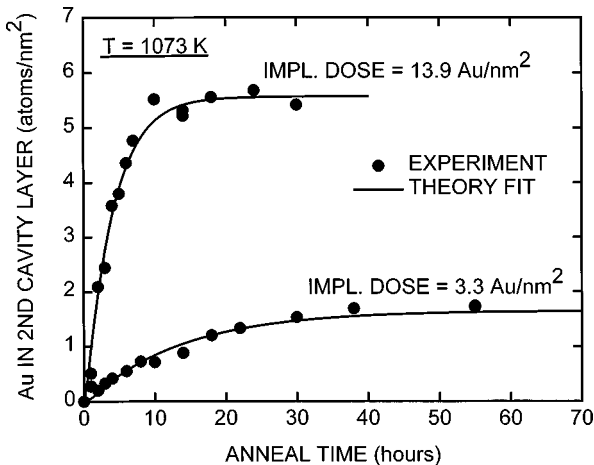

FIG. 6. Redistribution of Au from one cavity layer to another at 1073 K.

The areal density of Au in the second of the two cavity layers is plotted as a function of anneal time for all of the experiments in Figs. 5–7. In accord with Eqs. (9) and (10), the redistribution rate rises rapidly with temperature as a result of increases in both $D_{\mathrm{Au},i}$ and $[\mathrm{Au},i]_1$. The imbalance in the final partition of Au between the cavity layers is again apparent, as are its reduction with increasing temperature and its absence at the lower of the two Au doses. It is also noteworthy that the abrupt saturation seen in Fig. 2 for the dissolution of the precipitated Au-Si phase is not observed when Au is moving from one cavity layer to another; this is consistent with the continuous approach of $[\mathrm{Au},i]_1$ and $[\mathrm{Au},i]_2$ to each other and the resultant, more gradual decrease in Φ predicted by Eqs. (9) and (10). The detailed analysis of these data to obtain binding free energies is discussed in Sec. IV C.

C. Modeling and the extraction of binding free energies

The data in Figs. 2 and 5–7 were analyzed by numerically solving the more complete diffusion formalism described in Sec. II C and the Appendix and adjusting the desired binding free energies to produce agreement with experiment. The resulting values of ΔG are listed in Table I and plotted in Fig. 8. These quantities vary somewhat with temperature, which may result from the combined effects of (1) the entropy term $T\Delta S_{\mathrm{ex}}$ in Eq. (4), (2) changes in the chemisorbed

TABLE I. Binding free energies, cavity-trap areal densities, and related quantities.

Quantity	Temperature (K)	Value	Source
ΔG_{AuSi}	1023	2.33 eV	Fit in Fig. 2
ΔG_{AuSi}	1073	2.34 eV	Fit in Fig. 2
ΔG_{AuSi}	1123	2.31 eV	Fit in Fig. 2
ΔG_{AuSi}	1273	2.26 eV	Eq. (14) and $D_{\mathrm{Au},i}$
ΔG_{rc} for lower θ	1023	2.45 eV	Fit in Fig. 5
ΔG_{rc} for higher θ	1023	2.37 eV	Fit in Fig. 5
ΔG_{oc}	1023	2.55 eV	Fit in Fig. 5
ΔG_{rc} for lower θ	1073	2.48 eV	Fit in Fig. 6
ΔG_{rc} for higher θ	1073	2.31 eV	Fit in Fig. 6
ΔG_{oc}	1073	2.45 eV	Fit in Fig. 6
ΔG_{rc} for higher θ	1123	2.27 eV	Fit in Fig. 7
ΔG_{oc}	1123	2.39 eV	Fit in Fig. 7
$N_{\mathrm{Si}}[\mathrm{Au},i]_{\mathrm{AuSi}}D_{\mathrm{Au},i}$	1023	1.8×10^{5} mm^{-1} s^{-1}	Fit in Fig. 2
$N_{\mathrm{Si}}[\mathrm{Au},i]_{\mathrm{AuSi}}D_{\mathrm{Au},i}$	1073	6.4×10^{5} mm^{-1} s^{-1}	Fit in Fig. 2
$N_{\mathrm{Si}}[\mathrm{Au},i]_{\mathrm{AuSi}}D_{\mathrm{Au},i}$	1123	3.6×10^{6} mm^{-1} s^{-1}	Fit in Fig. 2
Trap areal density at 0.8 μm	1023	35 nm^{-2}	Fit in Fig. 2
Trap areal density at 0.8 μm	1073	32.5 nm^{-2}	Fit in Fig. 2
Trap areal density at 0.8 μm	1123	32 nm^{-2}	Fit in Fig. 2
Trap areal density at 0.3 and 0.9 μm	All	30 nm^{-2}	TEM, Ref. 32
θ_t	1023	0.11	Eq. (7)
θ_t	1073	0.18	Eq. (7)
θ_t	1123	$\gtrsim$0.2	Eq. (7)

state with temperature,[30] and (3) the specific choice of the diffusion prefactor discussed at the end of Sec. II B. The reason for high-dose and low-dose values of ΔG_{rc} being given is discussed below. The fits in Fig. 2 serve also to determine the product of the diffusion coefficient and the solid solubility of interstitial Au, and because this product governs Au transport under many circumstances of technological interest, we include its values in the table.

In the above model calculations, the initial concentration-versus-depth profile of the implanted Au was equated to a smoothed curve through the profile measured by RBS. The Au in the implanted layer was assumed to be in the form of precipitated Au-Si phase. In the case of the redistributions from the implanted layer to a single cavity layer shown in Fig 2, steps were taken to assure that the Au-Si phase was indeed present, as discussed in Sec. IV A; this matter was less consequential for the redistribution from one cavity layer to another, since in these experiments the implanted Au transferred rapidly to the first cavity layer. The concentration profiles of cavity-wall trap sites used in the model were derived from the implantation profiles of implanted He, as calculated using the Monte Carlo range code TRIM;[43] these profiles were rescaled slightly in depth to conform to the observed redistributions of the Au, and the concentration amplitudes were scaled so as to yield trap areal densities consistent with the saturation levels in Fig. 2 or with estimates based on TEM.[32] The trap areal densities employed are listed in Table I. Both external and cavity surfaces were taken to be sources for self-interstitials and vacancies, so that the concentrations of these point defects remained at their equilibrium values at such surfaces. The remaining parameters in the formalism were evaluated from independent information, as discussed in the Appendix.

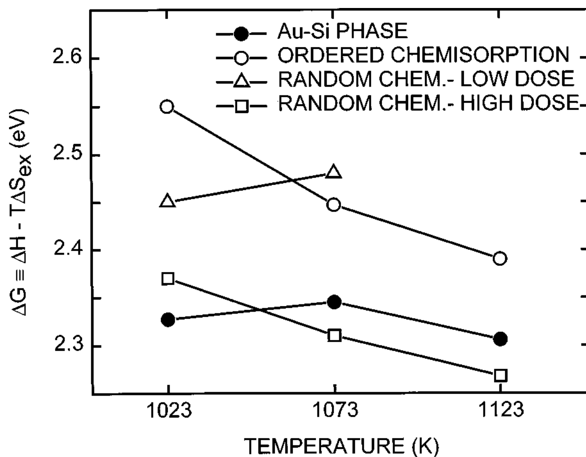

FIG. 8. Binding free energies of Au relative to interstitial solution.

The curves through the data in Figs. 2 and 5–7 show the results of the fitted model calculations. In Fig. 2, the rate of Au accumulation in the cavity layer before saturation is governed predominantly by ΔG_{AuSi}, since the binding within the cavity sinks is sufficiently stronger than in the Au-Si phase to make $[\mathrm{Au},i]_2$ in Eq. (1) substantially smaller than $[\mathrm{Au},i]_1$; consequently, the fitting of this accumulation rate was used to determine ΔG_{AuSi}. In Figs. 5 and 6, the rate of redistribution from the first to the second cavity layer for the smaller Au dose is inferred to occur with both θ_1 and θ_2 less than θ_t, so that fitting of the redistribution rate served to determine ΔG_{rc}. The final partition of Au between cavity layers at this lower dose was not adjustable; since $\theta_1 < \theta_t$ and

the areal density of cavity-wall traps was assumed to be the same in the two cavity layers, the formalism necessarily predicted an asymptotic condition with one-half of the Au in each layer. Finally, the curves for the higher implantation dose in Figs. 5–7 depend in a more complex way on the interplay of ΔG_{oc} and ΔG_{rc}. Since $\theta_1 > \theta_t$ at this dose, in the early stages of the redistribution, when θ_2 and hence $[\mathrm{Au},i]_2$ are small, the transfer rate is governed predominantly by ΔG_{oc}; at longer anneal times, however, as the increase in θ_2 causes $[\mathrm{Au},i]_2$ to approach $[\mathrm{Au},i]_1$, the influences of ΔG_{oc} and ΔG_{rc} on the rate are comparable. Moreover, the fraction of the Au that is ultimately transferred to the second cavity layer depends on the difference of these quantities through θ_t as given by Eq. (7). The deduced values of θ_t for the three anneal temperatures are given in Table I, with the result at 1173 K being less well determined because the experimentally measured partition between the two cavity layers is approaching equality.

In adjusting ΔG_{rc} to fit the data obtained at 1023 and 1073 K, we allowed this binding free energy to differ between the high-dose and low-dose cases. We considered this to be justified in view of the likelihood of multiple types of random-chemisorption sites with appreciably different binding free energies; in the presence of such a range of binding energies, the apparent binding energy would increase with decreasing θ as a result of preferential occupation of stronger sites. A more rigorous treatment would explicitly include a range of binding free energies, but, as discussed in Sec. II, we concluded that the available experimental data are insufficient to support such added complexity. As seen in Table I and Fig. 8, the fitted ΔG_{rc} do indeed differ somewhat between low and high dose, with a higher value at the lower dose as expected; while the difference of ~ 0.1 eV corresponds to a shift of only $\sim 5\%$, it translates via Eqs. (9) and (10) into a noticeable change in the rate of Au redistribution between layers.

As discussed in Sec. II B, our extraction of the binding free energies depends on independent knowledge of the diffusion coefficient of interstitial Au, for which precise data are unavailable. This, together with the approximation made in the modeling and the experimental uncertainties, are considered to result in an absolute uncertainty of approximately ± 0.3 eV in the reported energies. The relative energies of the various states are believed to be known with substantially less uncertainty, about ± 0.05 eV. The diffusivity-solubility product of interstitial Au given in Table I has an estimated uncertainty of $\pm 20\%$.

V. DISCUSSION

The cavity walls of the present investigation differ significantly from the external Au-chemisorbed surfaces of earlier studies[20–30] as a result of multiple cavity-wall orientations and perhaps also the small size of cavity features, $\lesssim 10$ nm. Nevertheless, it is illuminating to consider aspects of our findings in the light of a recently proposed surface phase diagram[30] based on external-surface experiments for the (111) orientation, the dominant one on cavity walls.[32,34,35] We begin by recalling that, when the total areal density of implanted Au in the present experiments was 14 nm^{-2}, the final partition of Au between two cavity layers departed sub-

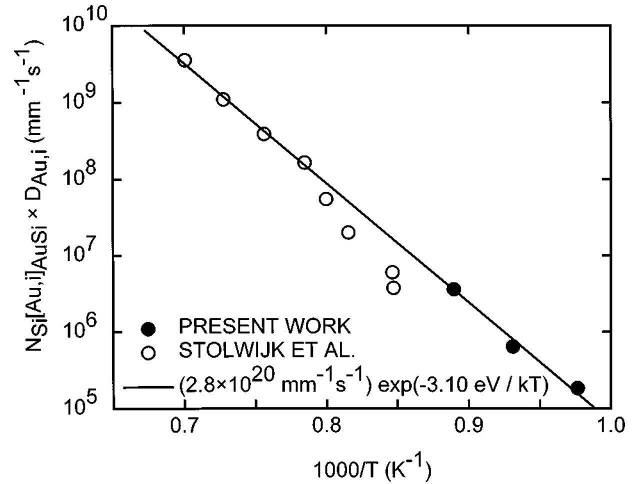

FIG. 9. Product of interstitial-Au solubility and diffusivity from the present work and from Ref. 2.

stantially from equality at 1023 K, slightly at 1073 K, and not detectably at 1123 K; in this case the condition of equal balance corresponded to $\theta \simeq 0.23$. As discussed in Sec. IV B, we interpret this asymptotic imbalance as indicating a two-phase surface condition in the first cavity layer. In comparison, for $\theta = 0.23$, the proposed surface phase diagram of Ref. 30 shows the two-phase condition giving way to a single, high-temperature, presumably disordered phase at about 1000 K. Thus, both our experiments and the external-surface studies point to an entropy-driven loss of order occurring in the vicinity of 1000 K.

A second finding in the present experiments was that, when the total areal density of implanted Au was about 3 nm^{-2}, the final partition between cavity layers was equal even at the lowest temperature of 1023 K; in this case, $\theta \simeq 0.05$ at the end of the experiment. This behavior does not conform to the proposed (111)-surface phase diagram at 1023 K, where the disordered, Au-containing phase is predicted to coexist with a Au-free, 7×7 Si surface for $\theta \lesssim 0.2$. Were such a two-phase condition present on the cavity walls, the considerations discussed in Secs. II and IV would predict the applicability of Eq. (6), rather than Eq. (5), and no redistribution of Au from one cavity layer to another. One plausible explanation for the disparity is simply that the cavity walls, with facet sizes $\lesssim 10$ nm, do not undergo the very complex and long-range 7×7 reconstruction that is thought to inhibit Au chemisorption and thereby necessitate the coexisting disordered phase for accommodation of the Au. In the absence of the 7×7 reconstruction, random-site chemisorption of Au can be expected to occur over the entire (111) surface, consistent with our experimental results and with Eq. (5). We conclude the discussion of this still-to-be-resolved matter by noting its particular significance for the extrapolation of our results into the regime of very small θ. Pending further information, we will treat this regime using Eq. (5).

The diffusivity-solubility product determined in this work is shown in Fig. 9 together with earlier, higher-temperature results.[2] Consistency between the two sets of data is seen to be good. This comparison is especially significant in view of the very different experimental approaches taken in the two studies: we used ion-implanted specimens, and we mea-

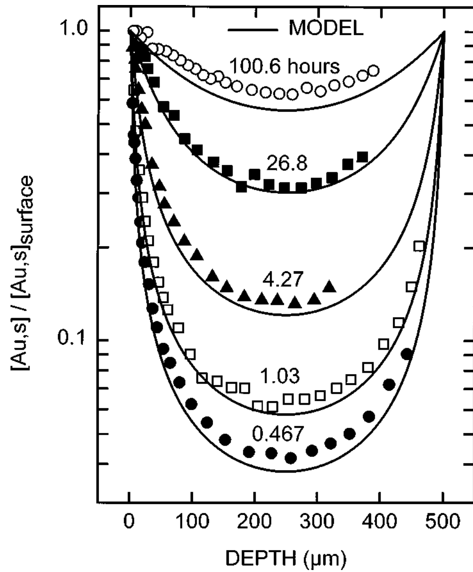

FIG. 10. Evolution of [Au,s] in the presence of surface Au-Si phase during annealing at 1273 K, as measured experimentally (Ref. 2) and as calculated using the theoretical model of the present work. The thickness of the specimen is 500 μm.

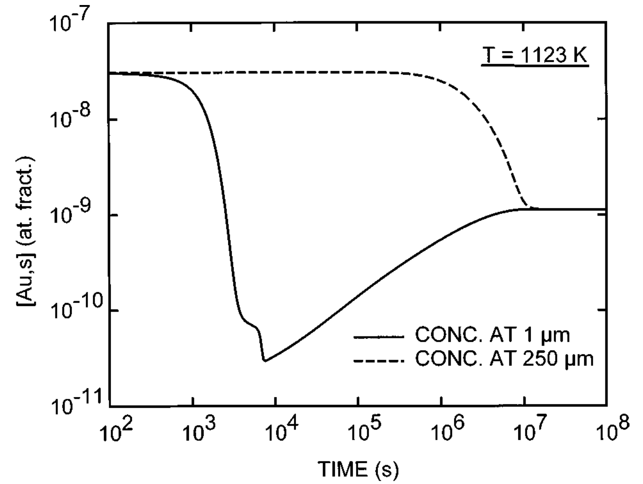

FIG. 11. Predicted time dependence of [Au,s] at 1123 K in the presence of cavity gettering.

sured the steady-state flow of interstitial Au from precipitated Au-Si phase to sinks over a submicrometer distance; in contrast, the earlier investigators employed evaporated Au as a source, and they used electrical measurements to profile the immobile, substitutional component of the Au over distances of hundreds of micrometers, with deliberately introduced dislocation sinks serving to remove excess Si self-interstitials and thereby maintain local equilibrium between the interstitial and substitutional Au. The combined results in Fig. 9 indicate that the diffusivity-solubility product for interstitial Au in Si is approximately given by

$$N_{\mathrm{Si}}[\mathrm{Au},i]_{\mathrm{AuSi}}D_{\mathrm{Au},i}=(2.8\times10^{20}\ \mathrm{mm}^{-1}\ \mathrm{s}^{-1})\times\exp(-3.10\ \mathrm{eV}/kT). \qquad (14)$$

The mathematical model of the Si-Au system and the associated parametrization that were introduced in Sec. II C and detailed in the Appendix are tested only partially by application to our experimental data. This is so because, as discussed in Sec. II C, the experiments were carried out under conditions where the conversion between mobile, interstitial Au and immobile, substitutional Au had little influence on the observed behavior. Consequently, as a further validation of the applicability of the model, we employed it with no change of parameter values to predict the depth-dependent accumulation of substitutional Au within dislocation-free Si having equilibrium Au-Si phase at the two opposing surfaces, under conditions conforming to published experimental data.[2] A comparison between the model predictions and the experimental data is shown in Fig. 10, and the agreement is seen to be good. Like earlier investigators,[1–7] we find that the predominant rate-controlling step in the buildup of substitutional Au is the diffusion to the surface of self-interstitial atoms formed when interstitial Au transforms to substitutional Au; the diffusion of interstitial Au from the surface source is so rapid that [Au,i] varies little through the specimen, and the relatively slow influx of vacancies from the surface contributes only slightly to the conversion from Au_i to Au_s.

The experimental results and theoretical modeling of the present work provide a basis for quantitative treatment of the gettering of Au impurities by cavities in Si. Significant features of such gettering are illustrated in Fig. 11. This plot shows the predicted influence of a cavity layer on the concentration of substitutional Au, the solute state predominantly affecting electrical properties, at a temperature of 1123 K. In the calculation, the Au was initially distributed uniformly through a 500-μm Si wafer; the starting atomic fractions of interstitial and substitutional Au were equated to the respective solubilities in equilibrium with the Au-Si phase at 1123 K, 4.5×10^{-11} and 3.0×10^{-8} atomic fraction. The cavity layer was located at a depth of 5 μm, and the associated areal density of chemisorption sites was taken to be 30 nm^{-2}, representative of the values deduced from the present experiments. Figure 11 shows the time dependence of [Au,s] at two depths: 1 μm, in the region where devices would be constructed, and 250 μm, in the center of the wafer.

The evolution of [Au,s] at 1 μm in Fig. 11 shows two distinct stages. For times $\lesssim10^4$ s, the movement of interstitial Au atoms to the cavity sinks induces a monotonic decrease in [Au,s], at a rate governed predominantly by the transport of Si interstitial atoms from the external surface and from cavity surfaces to accommodate the formation of mobile interstitial Au by the reaction of Eq. (12); the transport of the interstitial Au to the cavity sinks after its formation is relatively rapid and therefore not rate controlling. The decrease exhibits two substages, reflecting, respectively, the time for transport of Si interstitials from the surface to 1 μm and the time for transport of Si interstitials throughout the region between the surface and cavity layer. At longer times, as Au comes to the cavity sinks from progressively greater depths within the wafer, the value of [Au,i] adjacent to the cavities layer rises as a result of the θ dependence in Eq. (5), and this in turn causes [Au,s] at 1 μm to increase. Under the conditions of this calculation, the formation of interstitial Au deeper within the material is enabled not only by the aforementioned in-diffusion of Si interstitials but also, to a substantial degree, by the out-diffusion of vacancies formed

through the reaction of Eq. (11). At sufficiently long times, the system comes into equilibrium with the cavities, and [Au,s] and the other relevant concentrations become independent of depth.

Two features of the predicted behavior in Fig. 11 warrant emphasis because of their technological significance. First, cavity gettering is capable of reducing the concentration of Au far below its solubility; indeed, if the starting concentration in Fig. 11 is divided by any number >1, the predicted concentration-time curves are simply shifted downward on the logarithmic concentration scale with no significant distortion. The physical origin of this property is that, when random chemisorption of Au on cavity walls at small θ is in equilibrium with Au in solution, $[\mathrm{Au},s] \propto [\mathrm{Au},i] \propto \theta$. The second noteworthy feature is that, by choosing an intermediate anneal time to allow sufficient diffusion in the near-surface region while simultaneously minimizing θ, the Au concentration in the device-critical near-surface layer can be reduced substantially below the long-time, asymptotic value.

VI. CONCLUSION

By determining the binding free energies of Au on cavity walls, this study quantified the strength of a promising gettering reaction, and it achieved a significant step in establishing the energetics of Au on Si surfaces relative to the solution state. Remaining issues include (1) the partitioning of Au atoms among multiple chemisorption states at elevated temperatures, which was addressed here only in a preliminary way; (2) the separation of enthalpy and entropy contributions to the binding free energy; and (3) the variation of these properties with the crystallographic orientation of the surface. One potential avenue to such more detailed information is the performance of experiments analogous to those presented here, but with one or more cavity layers replaced with well characterized external surfaces of unique crystallographic orientation. Steps in this direction are already being taken for Cu on Si.[44]

The results of our experiments were incorporated with other information into a predictive mathematical model of Au transport and reactions in cavity-containing Si. This model quantitatively reproduces our data, and it is also in good agreement with other experiment results with which comparison was made. We believe the treatment to be capable of providing a realistic description of Au gettering under the more complicated conditions of technological interest.

ACKNOWLEDGMENTS

The authors benefited from a number of discussions with J. S. Williams, J. Wong-Leung, and W. R. Wampler. This work was supported by the U.S. Dept. of Energy, Office of Basic Energy Sciences, under Contract No. DE-AC04-94AL85000. Sandia National Laboratories is a multiprogram laboratory operated by Sandia Corporation, a Lockheed Martin Company, for the U.S. Department of Energy.

APPENDIX: DIFFUSION-REACTION FORMALISM AND PARAMETER VALUES

There are six relevant species whose concentrations vary with depth and time: mobile interstitial Au, essentially immobile substitutional Au, Au bound within precipitates of the Au-Si phase, Au chemisorbed on the walls of cavities, mobile Si self-interstitials, and mobile Si vacancies. The differential equations governing the concentrations are, respectively,

$$(\partial/\partial t)[\mathrm{Au},i] = D_{\mathrm{Au},i}(\partial^2/\partial x^2)[\mathrm{Au},i] - S_{\mathrm{AuSi}} - S_{\mathrm{cav}} + S_{\mathrm{Au\text{-}I}} - S_{\mathrm{Au}\text{-}V}, \tag{A1}$$

$$(\partial/\partial t)[\mathrm{Au},s] = -S_{\mathrm{Au}\text{-}I} + S_{\mathrm{Au}\text{-}V}, \tag{A2}$$

$$(\partial/\partial t)[\mathrm{Au,AuSi}] = S_{\mathrm{AuSi}}, \tag{A3}$$

$$(\partial/\partial t)[\mathrm{Au,cav}] = S_{\mathrm{cav}}, \tag{A4}$$

$$(\partial/\partial t)[I] = D_I(\partial^2/\partial x^2)[I] - S_{I\text{-}V} - S_{\mathrm{Au}\text{-}I}, \tag{A5}$$

$$(\partial/\partial t)[V] = D_V(\partial^2/\partial x^2)[V] - S_{I\text{-}V} - S_{\mathrm{Au}\text{-}V}. \tag{A6}$$

Here the D are diffusion coefficients, the bracketed expressions are concentrations expressed as atomic fraction, the source term S_{AuSi} takes account of the reaction of interstitial Au with Au-Si precipitates, S_{cav} treats the reaction with cavities, and the terms $S_{\mathrm{Au}\text{-}V}$, $S_{\mathrm{Au}\text{-}I}$, and $S_{I\text{-}V}$ reflect the reactions of Eqs. (11), (12), and (13), respectively. Using procedures and considerations discussed elsewhere,[45,46] these source terms are constructed in a manner appropriate for reversible, diffusion-limited reactions that approach equilibria specified by Eqs. (3)–(6) and by

$$[I] = \exp(-\Delta G_I/kT), \tag{A7}$$

$$[V] = \exp(-\Delta G_V/kT). \tag{A8}$$

The resulting source terms are

$$S_{\mathrm{AuSi}} = 4\pi D_{\mathrm{Au},i}\{R_{\mathrm{AuSi}}N_{\mathrm{AuSi}}(x)\}\{[\mathrm{Au},i] - \exp(-\Delta G_{\mathrm{AuSi}}/kT)\} \quad \text{for } [\mathrm{Au,AuSi}]>0, \tag{A9}$$

$$S_{\mathrm{cav}} = 4\pi D_{\mathrm{Au},i}N_{\mathrm{Si}}\{R_{\mathrm{cav}}/n_{\mathrm{cav}}\}([\mathrm{Au},i]\{A_{\mathrm{cav}}(x) - [\mathrm{Au,cav}]\} - [\mathrm{Au,cav}]\exp(-\Delta G_{\mathrm{rc}}/kT)) \quad \text{for } [\mathrm{Au,cav}]/A_{\mathrm{cav}} \leq \theta_t, \tag{A10a}$$

$$S_{\mathrm{cav}} = 4\pi D_{\mathrm{Au},i}N_{\mathrm{Si}}\{R_{\mathrm{cav}}/n_{\mathrm{cav}}\}\{[\mathrm{Au},i] - \exp(-\Delta G_{\mathrm{oc}}/kT)\} \quad \text{for } \theta_t \leq [\mathrm{Au,cav}]/A_{\mathrm{cav}} < 1, \tag{A10b}$$

$$S_{\mathrm{Au}\text{-}I} = 4\pi D_I N_{\mathrm{Si}} R_{\mathrm{Au}\text{-}I}\{[\mathrm{Au},s][I] - [\mathrm{Au},i]\exp(-\Delta G_{\mathrm{Au}\text{-}I})\}, \tag{A11}$$

$$S_{\mathrm{Au}\text{-}V} = 4\pi\{D_{\mathrm{Au},i} + D_V\}N_{\mathrm{Si}}R_{\mathrm{Au}\text{-}V}\{[\mathrm{Au},i][V] - [\mathrm{Au},s]\exp(-\Delta G_{\mathrm{Au}\text{-}V})\}, \tag{A12}$$

$$S_{I\text{-}V} = 4\pi\{D_I + D_V\}N_{\mathrm{Si}}R_{I\text{-}V}([I][V] - \exp\{-(\Delta G_I + \Delta G_V)/kT\}). \tag{A13}$$

TABLE II. Additional parameters evaluated from independent information.

Parameter	Value	Source
$D_{\mathrm{Au},i}$	$(0.1\ \mathrm{mm^2/s})\exp(-0.4\ \mathrm{eV}/kT)$	See Sec. II B
D_I	$(20\ \mathrm{mm^2/s})\exp(-1.2\ \mathrm{eV}/kT)$	Ref. 3
D_V	$(100\ \mathrm{mm^2/s})\exp(-0.4\ \mathrm{eV}/kT)$	Representative value, Ref. 48
ΔG_I	$3.8\ \mathrm{eV}-9.9\ kT$	Ref. 3
ΔG_V	$4.2\ \mathrm{eV}-3.7\ kT$	Ref. 3 with above D_V
R_{AuSi}	1 nm	Order-of-magnitude estimate
$N_{\mathrm{AuSi}}(x)$	Chosen to reproduce initial [Au,AuSi]	RBS analysis
R_{cav}	10 nm	Ref. 32
n_{cav}	10^4	10-nm cavity with monolayer wall coverage
$R_{\mathrm{Au\text{-}I}}$	1 nm	Order-of-magnitude estimate
$R_{\mathrm{Au\text{-}}V}$	1 nm	Order-of-magnitude estimate
$R_{I\text{-}V}$	1 nm	Order-of-magnitude estimate

Here the R are effective reaction radii, N_{AuSi} is the number of Au-Si precipitates per unit volume, N_{Si} is the atomic density of Si, n_{cav} is the number of chemisorbed Au atoms per cavity when $\theta=1$, and A_{cav} is the concentration of Au atoms bound to cavities when $\theta=1$, expressed as atomic fraction. Although R_{AuSi} varies with changes in [Au, AuSi], this effect is inconsequential in the present context and is neglected. A superficial difference in nomenclature from Refs. 45 and 46 is that the entropy-related prefactors of Boltzmann factors have been incorporated into the temperature-dependent binding free energies ΔG. In order to accommodate numerical solution of this formalism, the above source terms were altered as discussed elsewhere[46] to produce slight rounding wherever there is a discontinuity in a first derivative. The method of numerical solution has been described elsewhere.[45,47]

Table II lists the values and sources of parameters that were not determined in the present study. The reaction radii are the least critical quantities. This is so because the physical system evolves during annealing with local near-equilibrium among the reacting species at any given depth, and the radii influence only the approach to that local equilibrium; as a result, even order-of-magnitude changes in the radii are found to be inconsequential for predicting observable properties. Hence, very rough estimates of these quantities were deemed sufficient. It should also be noted that, for our experiments and also for others dealing with Au in Si of which we are aware, the experimentally measured properties are determined predominantly by products of diffusion coefficients with equilibrium concentrations of the mobile species, rather than by the values of the individual factors. As a result, for example, $D_I\exp(-\Delta G_I/kT)$, $D_V\exp(-\Delta G_V/kT)$, and $D_{\mathrm{Au},i}\exp(-\Delta G_{\mathrm{AuSi}}/kT)$ are known much more accurately than their individual factors. (See, e.g., Ref. 1.) Consequently, in assigning parameter values, we sought particularly to be consistent with the best available information on the products. The choice for $D_{\mathrm{Au},i}$ was discussed in Sec. II B.

[1] U. M. Gösele and T. Y. Tan, in *Materials Science and Technology, Vol. 4: Electronic Structure and Properties of Semiconductors*, edited by W. Schröter (VCH, New York, 1991), pp. 197–247.

[2] N. A. Stolwijk, J. Hölzl, W. Frank, E. R. Weber, and H. Mehrer, Appl. Phys. A: Solids Surf. **39**, 37 (1986).

[3] F. F. Morehead, in *Defects in Electronic Materials*, edited by M. Stavola, S. J. Pearton, and G. Davies, MRS Symposia Proceedings No. 104 (Materials Research Society, Pittsburgh, 1988), p. 99.

[4] S. Coffa, L. Calcagno, S. U. Campisano, G. Calleri, and G. Ferla, J. Appl. Phys. **64**, 6291 (1988).

[5] C. Boit, F. Lau, and R. Sittig, Appl. Phys. A: Solids Surf. **50**, 197 (1990).

[6] D. Mathiot, Phys. Rev. B **45**, 13 345 (1992).

[7] M. Morooka, Jpn. J. Appl. Phys., Part 1 **35**, 2537 (1996).

[8] K. Graff, *Metal Impurities in Silicon-Device Fabrication* (Springer, Berlin, 1995), pp. 105–110.

[9] D. A. Pietila and D. B. Masson, J. Electrochem. Soc. **135**, 686 (1988).

[10] E. Ö. Sveinbjörnsson, O. Engström, and U. Södervall, J. Appl. Phys. **73**, 7311 (1993).

[11] F. Gaisenau and W. Schröter, J. Electrochem. Soc. **143**, 361 (1996).

[12] T. E. Seidel, R. L. Meek, and A. G. Cullis, J. Appl. Phys. **46**, 600 (1975).

[13] W. Skorupa, R. Kögler, K. Schmalz, and H. Bartsch, Nucl. Instrum. Methods Phys. Res. B **55**, 224 (1991).

[14] D. Jaworska and E. Tarnowska, J. Phys. D **26**, 2226 (1993).

[15] A. Grob, P. Rohr, G. Mariani, J. Sevely, and J. J. Grob, Nucl. Instrum. Methods Phys. Res. B **112**, 169 (1996).

[16] J. Wong-Leung, J. S. Williams, R. G. Elliman, E. Nygren, D. J. Eaglesham, D. C. Jacobson, and J. M. Poate, Nucl. Instrum. Methods Phys. Res. B **96**, 253 (1995).

[17] J. Wong-Leung, E. Nygren, and J. S. Williams, Appl. Phys. Lett. **67**, 416 (1995).

[18] J. Wong-Leung, J. S. Williams, and E. Nygren, Nucl. Instrum. Methods Phys. Res. B **106**, 424 (1995).
[19] S. M. Myers and G. A. Petersen, in *Ion-Solid Interactions for Materials Modification and Processing*, edited by D. B. Poker *et al.*, MRS Symposia Proceedings No. 396 (Materials Research Society, Pittsburgh, 1996), p. 733.
[20] G. Le Lay, M. Manneville, and R. Kern, Surf. Sci. **65**, 261 (1977).
[21] A. A. Baski, J. Nogami, and C. F. Quate, Phys. Rev. B **41**, 10 247 (1990).
[22] J. Nogami, A. A. Baski, and C. F. Quate, Phys. Rev. Lett. **65**, 1611 (1990).
[23] T. Hasegawa, K. Takata, S. Hosaka, and S. Hosoki, J. Vac. Sci. Technol. A **8**, 241 (1990).
[24] W. Swiech, E. Bauer, and M. Mundschau, Surf. Sci. **253**, 283 (1991).
[25] Y. Yamamoto, Surf. Sci. **271**, 407 (1992).
[26] X. F. Lin, K. J. Wan, J. C. Glueckstein, and J. Nogami, Phys. Rev. B **47**, 3671 (1993).
[27] L. D. Marks and R. Plass, Phys. Rev. Lett. **75**, 2172 (1995).
[28] R. Plass and L. D. Marks, Surf. Sci. **342**, 233 (1995).
[29] T. Hasegawa, S. Hosoki, and K. Yagi, Surf. Sci. **355**, L295 (1996).
[30] R. Plass and L. D. Marks, Surf. Sci. **380**, 497 (1997).
[31] C. C. Griffioen, J. H. Evans, P. C. De Jong, and A. Van Veen, Nucl. Instrum. Methods Phys. Res. B **27**, 417 (1987).
[32] D. M. Follstaedt, S. M. Myers, G. A. Petersen, and J. W. Medernach, J. Electron. Mater. **25**, 151 (1996).
[33] *Binary Alloy Phase Diagrams*, edited by J. L. Murray, L. H. Bennett, and H. Baker (ASM, Metals Park, OH, 1986), Vol. 1, pp. 312 and 313.
[34] D. M. Follstaedt, Appl. Phys. Lett. **62**, 1116 (1993).
[35] D. J. Eaglesham, A. E. White, L. C. Feldman, N. Moriya, and D. C. Jacobson, Phys. Rev. Lett. **70**, 1643 (1993).
[36] S. M. Myers, G. A. Petersen, and C. H. Seager, J. Appl. Phys. **80**, 3717 (1996).
[37] W. R. Wilcox and T. J. LaChapelle, J. Appl. Phys. **35**, 240 (1964).
[38] R. N. Hall and J. H. Racette, J. Appl. Phys. **35**, 379 (1964).
[39] M. K. Bakhadyrkhanov, S. Zainabidinov, and A. Khamidov, Fiz. Tekh. Poluprovodn. **14**, 412 (1980) [Sov. Phys. Semicond. **14**, 243 (1980)].
[40] E. R. Weber, in *Properties of Silicon, EMIS Datareviews Series No. 4* (INSPEC, New York, 1988), pp. 409–451.
[41] W.-K. Chu, J. W. Mayer, and M.-A. Nicolet, *Backscattering Spectrometry* (Academic, New York, 1978).
[42] J. F. Ziegler, *Helium Stopping Powers and Ranges in All Elements* (Pergamon, New York, 1977).
[43] J. F. Ziegler, J. P. Biersack, and U. Littmark, *The Stopping and Range of Ions in Solids* (Pergamon, New York, 1985).
[44] W. R. Wampler, in *Control of Semiconductor Surfaces and Interfaces*, edited by S. M. Prokes *et al.*, MRS Symposia Proceedings No. 448 (Materials Research Society, Pittsburgh, 1997), p. 371.
[45] S. M. Myers, P. M. Richards, W. R. Wampler, and F. Besenbacher, J. Nucl. Mater. **165**, 9 (1989).
[46] S. M. Myers and D. M. Follstaedt, J. Appl. Phys. **79**, 1337 (1996).
[47] S. M. Myers, D. E. Amos, and D. K. Brice, J. Appl. Phys. **47**, 1812 (1976).
[48] K. V. Ravi, in *Properties of Silicon* (Ref. 40), pp. 256 and 257.